Boletim da Sociedade Astronômica Brasileira, **34**, no. 1, 295-299

Modelling the strong Fe II emission

Simultaneous photoionization modelling in optical and NIR

D. Dias dos Santos[1], S. Panda[2], A. Rodríguez-Ardila[2,1], & M. Marinello[2]

[1] Divisão de Astrofísica, Instituto Nacional de Pesquisas Espaciais, Avenida dos Astronautas 1758, São José dos Campos, 12227-010, SP, Brazil. e-mail: denimara.santos@inpe.br
[2] Laboratório Nacional de Astrofísica - Rua dos Estados Unidos 154, Bairro das Nações. CEP 37504-364, Itajubá, MG, Brazil

Abstract. Constraining the physical conditions of the ionized media in the vicinity of an active supermassive black hole (SMBH) is crucial to develop our understanding of how these complex systems operate. Metal emission lines such as iron (Fe) are useful probes to trace the abundance, activity, and evolution of the gaseous media in these accreting systems. Among these, the Fe II emission has been the focus of many prior studies to investigate the energetics, kinematics and composition of the broad-emission line region (BLR) from where these emission lines are produced. In this work, for the first time, we present the simultaneous Fe II modeling in the optical and near-infrared (NIR) region. We use CLOUDY photoionization code to simulate both spectral regions in the wavelength interval 4000-12000 Å and analyze the results for two Fe II atomic datasets implemented in CLOUDY. We compare our model predictions with the observed line intensity ratios for I Zw 1 - a prototypical strong Fe II-emitting AGN. This allows putting constraints on the BLR cloud density and metal content that is optimal for the production of the Fe II emission. As a first test, we examine how the emission is impacted under low column density conditions in the BLR - 10^{22} cm^{-2} and 10^{23} cm^{-2}. From the comparison between models and observations, we found that the NIR and optical Fe II strength observed in I Zw 1 can be predicted by gas with the column density of 10^{23} cm^{-2} and cloud densities above 10^{10} cm^{-3} and abundance $2\,Z_{\odot} \leq Z \leq 5\,Z_{\odot}$. We conclude that simultaneous modeling in the optical and NIR is essential to put firm constraints in the obtained physical conditions for reproducing the Fe II emission, breaking possible degenerate solutions from the simulations.

Resumo. Restringir as condições físicas do meio ionizado próximo de um buraco negro supermassivo ativo (SMBH) é crucial para desenvolver nossa compreensão de como tais sistemas complexos funcionam. Linhas de emissão de metais como ferro (Fe) são úteis para rastrear a abundância, atividade e evolução de meios gasosos nesses sistemas de acreção. Dentre estas, a emissão Fe II tem sido foco de diversos estudos anteriores para investigar a energia, cinemática e composição da região emissora de linhas largas (BLR), de onde essas linhas de emissão são produzidas. Neste trabalho, pela primeira vez, apresentamos a modelagem simultânea do Fe II na região do óptico e infravermelho próximo (NIR). Usamos o código de fotoionização CLOUDY para simular ambas regiões espectrais no intervalo de comprimento de onda 4000-12000 Å e analisamos os resultados para dois conjuntos de dados atômicos de Fe II implementados no CLOUDY. Comparamos nossas previsões do modelo com as razões de intensidades das linhas observadas em I Zw 1 - um protótipo de AGN forte emissor de Fe II. Isso permite colocar restrições na densidade da nuvem da BLR e no teor de metal que favorece a produção da emissão de Fe II. Como um primeiro teste, nós examinamos como a emissão é impactada sob condições de baixa densidade de coluna na BLR - 10^{22} cm^{-2} and 10^{23} cm^{-2}. A partir da comparação entre os modelos e observações, descobrimos que a intensidade do Fe II observado em I Zw 1, pode ser previsto por um gás com densidade de coluna de 10^{23} cm^{-2} e densidades acima de 10^{10} cm^{-3} em nuvens com metalicidade $2\,Z_{\odot} \leq Z \leq 5\,Z_{\odot}$. Concluímos que a modelagem simultânea no óptico e NIR é essencial para colocar firmes restrições nas condições físicas obtidas para reproduzir a emissão Fe II, quebrando possíveis soluções degeneradas das simulações.

Keywords. Galaxies: active – quasars: emission lines – Radiation mechanisms: thermal – Radiative transfer – Methods: data analysis

1. Introduction

Active Galactic Nuclei (AGNs) are embedded at the core of galaxies and contain an active supermassive black hole (SMBH) at their very centers. Radiation originates from the heating of matter that gets accreted onto the SMBH and then ionizes the gas and metal-rich media in the vicinity of these systems (Netzer 2015; Padovani et al. 2017). Due to their extended geometry, AGNs can look different based on the orientation that they are viewed from Collin et al. 2006; Panda et al. 2019. This effect also manifests in their observed spectra. Sources that exhibit both broad (permitted and semi-permitted) and narrow forbidden emission line profiles are classified as Type I, whereas the sources where no broad emission lines are perceived are grouped under Type II. In this work, we focus only on Type I sources and their emission. The origin of the broad emission lines is from a region that lies ∼0.01-0.1 parsec from the central ionizing source, and this distance is obtained using the well-known reverberation mapping technique applied to over 100 of AGNs to date (Blandford & McKee 1982; Peterson et al. 2004; Bentz et al. 2013; Du et al. 2015; Grier et al. 2017; Panda et al. 2019). This region, the broad line region (BLR), is responsible for the bulk of the emission that is observed in a typical Type I AGN spectrum (Berk et al. 2001; Glikman et al. 2006). One such prominent emission feature is the Fe II emission, which spans from the ultraviolet (UV) to near-infrared (NIR) regime (Wills et al. 1985; Verner et al. 1999; Marinello et al. 2020).

The Fe II emission mimics a continuum due to the accumulation of hundreds of thousands of transitions (>344,000) and thus is referred to as a pseudo-continuum (Verner et al. 1999; Sigut & Pradhan 2003). These numerous emissions from the Fe II ion are important to characterize the energy budget of the BLR, where ∼25% of the entire emission from the BLR is produced by the Fe II lines (Wills et al. 1985). Other studies have realized that the Fe II emission can be

used as a proxy to measure the relative abundance of metals in the BLR in AGNs across a wide range in redshift, thereby allowing us to understand the evolution of the metals in these galaxies (Hamann & Ferland 1992; Baldwin et al. 2004; Panda et al. 2019; Martínez-Aldama et al. 2021; Sarkar et al. 2021).

Another vital contribution of the Fe II-based studies has been the realization of templates for the Fe II emission. From the observational point of view, Boroson & Green 1992 were the first to extract the Fe II emission from a prototypical AGN Fe II emitter – I Zw 1. The Fe II template was prepared by removing all emission lines different from those of Fe II. This template approach is employed until today in several works to measure the Fe II optical intensity. In the UV advances were made by Vestergaard & Wilkes 2001 using high-quality spectrum extending the template method into the UV regime.

Since then, other works have also successfully produced different templates to quantify the UV-optical Fe II emission in large samples of AGNs (Tsuzuki et al. 2006; Kovačević-Dojčinović & Popović; Dong et al. 2010; Dong et al. 2011; Kovačević et al. 2010). Kovačević et al. 2010 developed a new optical Fe II template through the measurement of the individual Fe II multiplets groups, resulting in a better Fe II intensity ratio. Still, modeling the Fe II emission in I Zw 1-like sources has been a challenge because the traditional template unable to reproduce some features in the observed spectra. Recently, Park et al. 2022 proposed a new template generated from the observed spectrum of Mrk 493 for better modeling of the Fe II emission in I Zw 1-like sources.

Sigut & Pradhan 1998 and Sigut & Pradhan 2003 made advances in NIR predictions of Fe II spectra by using the Lyα fluorescence excitation mechanism to explain Fe II emission within, 8500–9500 Å. The Lyman process is solely responsible for exciting energy levels up to 13 eV and producing the emission lines in this region, confirmed from observations by Rodriguez-Ardila et al. 2002. The first semi-empirical Fe II template in the NIR was derived by Garcia-Rissmann et al. 2012 (hereafter GR) using an observed spectrum of I Zw1 supplemented with theoretical models (Sigut & Pradhan 1998; Sigut & Pradhan 2003; Sigut et al. 2004). Marinello et al. 2016; Marinello et al. 2020 successfully modeled the Fe II in the optical and NIR for 26 AGNs

Notably, the NIR spectrum shows Fe II emission lines isolated or semi-isolated, unlike in the UV-optical region, which allows for a better and more accurate determination of the line properties (see Figure 1). The Fe II lines around the 1-micron region at λ9997, λ10502, λ10863 and λ11127 are the most intense among the Fe II lines (Rudy et al. 2000; Rodriguez-Ardila et al. 2002; Riffel et al. 2006).). Recent work by Marinello et al. 2016 has shown that Fe II emission in the optical and near-infrared are intrinsically correlated. The complexity of the Fe II ion, combined with the difficulty of modeling its emission, has inspired authors (Martínez-Aldama et al. 2015; Panda et al. 2020)) to search for alternative approaches to study the Fe II emitting gas. Results from observational and photoionization modeling suggest that less complex ions, e.g., Ca II triplet (centered at λ8550, CaT) and the O I λ8446, λ11287, can be used as proxies for exploring the location of Fe II emitting gas (Marinello et al. 2016; Rodriguez-Ardila et al. 2002; Martínez-Aldama et al. 2015; Panda et al. 2020)).

Boroson & Green 1992 pioneered the efforts to understand the Fe II emission by showing that the strength of Fe II strongly correlates with other BLR and Narrow Line Region (NLR) properties. They used Principal Component Analysis (PCA), a mathematical technique, where the primary driver of their sample - Eigenvector 1 (EV1), reveals the anti-correlation between the peak intensity of [OIII]λ5007 and the optical Fe II within 4434-4684 Å centered at 4570 Å. Also, Boroson & Green 1992 found that there is a significant correlation between the peak [O III] intensity and the FWHM(Hβ). This then led to the FWHM(Hβ) vs. R_{FeII} connection, which is a well known optical plane of the quasar main sequence (Sulentic et al. 2000; Shen & Ho 2014; Marziani et al. 2018). In this context, the Fe II emission is an important parameter to determine the true drivers behind the EV1 (Panda et al. 2017; Panda 2021). Furthermore, the Fe II study is essential to understand the physical conditions of the BLR low-ionization line emitting gas, such as the metal content and density, and how they vary along the EV1.

The Fe II emission has been shown to be dependent on the BLR temperature and gas density, and also on other parameters such as composition and Brownian motion within the BLR cloud - high temperature (~5000-10000 K), relatively high density (log n_H = 10-12 cm^{-3}), super-solar abundances and microturbulence of the order of ~100 km s^{-1} have been shown to positively impact the production of the Fe II emission, especially in the UV and optical (Baldwin et al. 2004; Bruhweiler & Verner 2008; Panda et al. 2018; Panda et al. 2019). Thus, it is important to check the validity of these results in the NIR region which is the goal of this project.

In this work, we model the Fe II emission to understand the line formation and the nature of the physical conditions in AGN with strong Fe II emission. We model the optical and NIR Fe II simultaneously, in order to explore the BLR column density threshold required to reproduce the observable Fe II emission intensity. To this purpose, we compare photoionization model predictions with the observed estimates for the Fe II in the optical and NIR spectra of the I Zw 1. Section 2 presents the observational data for I Zw 1. Section 3 describes the modeling setup using the photoionization code CLOUDY. Preliminary results are highlighted and further discussions are made in Section 4. We summarize our findings from this study in Section 5.

2. I Zw1 the prototypical Fe II emitter

The Seyfert galaxy, I Zwicky 1 (I Zw1) at z= 0.061, has been considered a prototypical Fe II emitter, and widely studied in the literature (Wills et al. 1985; Rudy et al. 2000; Vestergaard & Wilkes 2001; Veron-Cetty et al. 2004; Huang et al. 2019). The object is classified as a Narrow-line Seyfert 1 galaxy (NLSy1), a subclass of Type-I AGNs which show FWHM(Hβ) < 2000 km s^{-1} and the flux ratio, [O III]λ5007/Hβ < 3 (Osterbrock et al. 1985).

More recently, the object has a reverberation mapping measurement of the distance of the line-emitting BLR from the central ionizing source, R_{BLR} = 37.2 light-days (Huang et al. 2019). This is particularly useful for us because the BLR radius is a key element in order to minimize the number of free parameters in our models.

The NIR spectrum was observed using the 3.2 m IRTF telescope (NASA Infrared Telescope Facility) at Mauna Kea, Hawaii-USA in 2000. It employed a SpeX spectrograph in cross dispersion mode (SXD) covering 0.8 – 2.4 μm, and photometric bands zJHK, with a spectral resolution of 2000 corresponding to the 0.8" × 15" slit. Rodriguez-Ardila et al. 2002 and Riffel et al. 2006). presented, in detail, the observational and data reduction information for the spectrum. The optical counterpart region was available through private communication, and it was published in Rodriguez-Ardila et al. 2002. The

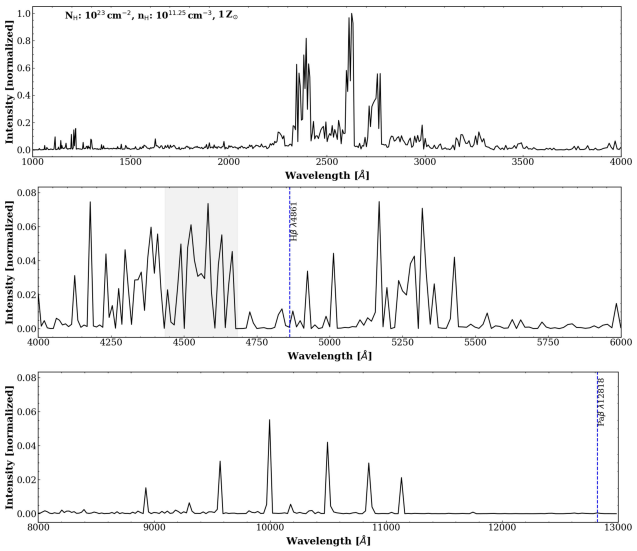

Figure 1. The Fe II emitted spectrum for an optically thin photoionized cloud with cloud density, n_H=$10^{11.25}$ cm^{-3} having solar abundances for column density case 10^{23} cm^{-2}. The optical Fe II range 4434-4684Å is highlighted in gray. We normalized the intensity of the Fe II emission by the maximum value for the entire simulated spectrum with a factor of 3.386×10^{7} erg cm^{-2} s^{-1}. The pseudo-continuum was constructed using Smyth et al. 2019 Fe II dataset.

spectrum was obtained at the CASLEO Observatory (Complejo Astronómico el Leoncito - San Juán, Argentina), employing the REOSC spectrograph in long slit mode covering the range 3500 – 6800 Å.

From these spectra, we obtain the optical Fe II and NIR intensities: $R_{4570} = 1.619 \pm 0.06$ and $R_{1\mu m} = 0.72 \pm 0.05$, respectively (2).

3. Photoionization modelling

We perform simulations of the Fe II spectrum using CLOUDY v17.03 (Ferland et al. 2017) using input parameters to generate the simulated models. We use the luminosity at 5100 Å $L_{5100} = 3.19\times10^{44}$erg s^{-1} from Kaspi et al. 2000, and the BLR radius measured by reverberation mapping $R_{BLR} = 37.2$ light-days from Huang et al. 2019, to limit the number of free parameters reducing to three. The free parameters are (i) the cloud column density $N_H = 10^{22}$ cm^{-2}, and 10^{23} cm^{-2}, (ii) the cloud mean hydrogen density $n_H = 10^7 - 10^{14}$ cm^{-3}, and (iii) the metal content (in the unit of $Z_\odot$) $0.1 \leq Z \leq 10$, which are estimated using the *GASS10* module (Grevesse et al. 2011)[1]. We assume the spectral energy distribution for I Zw 1 from Panda et al. 2020). A more complete description of the assumed range of the physical conditions incorporated in the photoionization models can be found in past studies (Panda et al. 2018; Panda et al. 2019; Panda et al. 2020)). The default model for the Fe II ion in CLOUDY is the one defined by Verner et al. 1999.

In addition, we use the developmental version of CLOUDY and incorporate the modelling setup as described above. The main difference between this version and the publicly available version (v17.03) of CLOUDY (Ferland et al. 2017) is the inclusion of alternate Fe II atomic datasets apart from the default one from Verner et al. 1999. This allows us to evaluate the performance of the existing Fe II datasets to recover, primarily, the intensities of the Fe II emission lines around 1-micron. The comparison of the simulated Fe II spectrum (or pseudo-continuum) in intensity units for the default (Verner et al. 1999) and for the new atomic database Smyth et al. 2019 is shown in Figure 2 for a representative hydrogen density ($n_H = 10^{11.25}$ cm^{-3}). We clearly see the improvement going from Verner et al. 1999 model (in red) to Smyth et al. 2019 (in blue) where the latter is able to recover the peak intensities similar to the observed value from Garcia-Rissmann et al. 2012. In reality, one needs to account for the line broadening wherein we broaden the synthetic spectrum with a suitable FWHM appropriate for the given source. This will be accounted for in our forthcoming work.

[1] The total number of models, therefore, is: N_H (3) × n_H (29) × Z (7) = 609.

4. Analysis and Results

We estimate the optical Fe II ratio R_{4570} and the NIR Fe II ratio $R_{1\mu m}$ from the outputs of our CLOUDY models. Here, the R_{4570} represents the ratio between the flux of optical Fe II centered at 4570Å to the flux of Hβ. While, the $R_{1\mu m}$ is the ratio of the sum of the fluxes from the 4 prominent Fe II lines at λ 9997, λ 10502, λ 10863 and λ 11127 to the flux of the Paβ. This is shown in Figure 3 for the column density case 10^{23} cm^{-2} utilizing the Smyth et al. 2019 Fe II dataset.

The diagnostic diagrams obtained for $R_{1\mu m}$ and R_{4570} versus the cloud density (n_H) and color-coded by abundances in solar values, are shown in Figure 4. For this work, we focus on the results obtained from Smyth et al. 2019 atomic dataset because, compared to Verner et al. 1999, is the best dataset that reproduces the strong Fe II emission for the parameters relevant for I Zw 1. We compare our obtained NIR and optical intensity from CLOUDY with the observed values respectively, $R_{1\mu m} = 0.72 \pm 0.05$ and $R_{4570} = 1.619 \pm 0.06$ (2) in Figure 4. For column density case of 10^{22} cm^{-2} the Fe II strength in the NIR is not reproduced even for abundances as high as 10x the solar values, although in the optical, the observed ratio can be achieved only for the models with $10\,Z_\odot$. Low column densities imply smaller clouds, and previous studies have shown that the Fe II emission originates from a region much deeper in the BLR cloud (Barth et al. 2013; Hu et al. 2008) later confirmed by photoionization models (Panda et al. 2018; Panda 2021). The combination of the two features limits the overall Fe II emission in the low column density case. On the other hand, for column density 10^{23} cm^{-2}, the R_{4570} ratio is reproduced but requires a high abundance up to $5\,Z_\odot$ while, in the case of the NIR $R_{1\mu m}$ ratio, is slightly lower (up to $2\,Z_\odot$). Besides that, the result is important to understand the column density threshold for Fe II formation in AGNs with strong Fe II emission. However, these results under low column densities are interesting to study lower Fe II sources, e.g., Population B sources in the EV1 context (Korista et al.2000; Korista et al. 2014; Panda et al. 2022).

We also estimate the cloud densities from our modelling based on the recovery of the optical and NIR Fe II intensity ratios. Focusing on the cloud column density case, $N_H = 10^{23}$ cm^{-2}, the range of cloud densities for the optical: $10^{10.6}$ - $10^{12.4}$ cm^{-3}, while for the NIR: 10^{10} - $10^{11.9}$ cm^{-3}. This suggests that the density associated with the two emissions are overlapping.

Our results have shown the potential to study in detail the NIR Fe II emission in strong Fe II emitters, and in general for all Type-I AGNs. As mentioned above, the NIR is more suitable for Fe II study than optical and UV. A more detailed analysis will be shown in a forthcoming work.

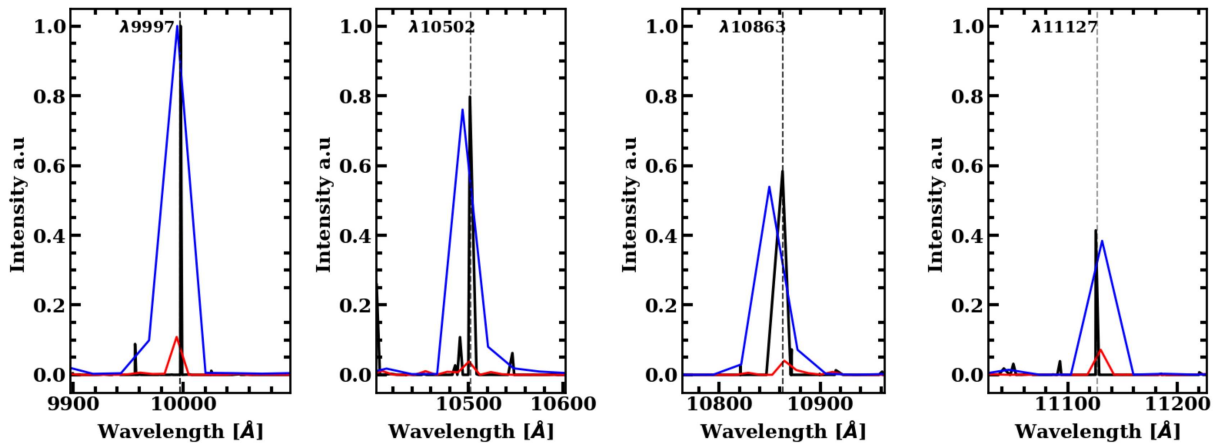

Figure 2. Predicted pseudo-continuum for Fe II emission for n_H=$10^{11.25}$ cm^{-3} using solar abundances for column density case 10^{23} cm^{-2}. The atomic databases Garcia-Rissmann et al. 2012, Verner et al. 1999, and Smyth et al. 2019, respectively are in colors black, red and blue.

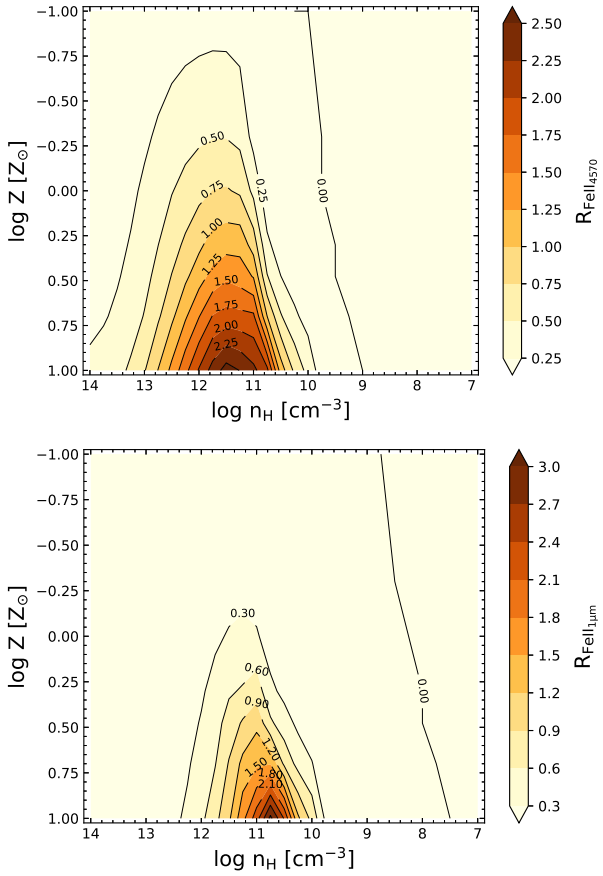

Figure 3. 2D histograms for the optical Fe II flux strength (i.e., R_{4570}, upper panel), and for the NIR Fe II flux strength (i.e., $R_{1\mu m}$, lower panel). The x and y axes for each panel are BLR cloud density (n_H) and BLR abundance (Z) in the log-scale, respectively. The color bar and contours (in black) represent the respective Fe II strengths. These models assume a column density, $N_H = 10^{23}$ cm^{-2}, and utilize the Smyth et al. 2019 Fe II atomic dataset.

5. Conclusion

In this work, for the first time, we explore the photoionization modeling using CLOUDY focusing on the simultaneous recovery of the optical and NIR Fe II emission for a prototypical Fe II-emitting AGN - I Zw 1. We probe a wide parameter space which includes the BLR cloud density (n_H), metal abundance in the BLR cloud, and the cloud column density -which then relates to the size of the BLR cloud. This allows us to recover the Fe II intensity ratios in the optical (R_{4570}) and NIR ($R_{1\mu m}$). We briefly summarize the results of this work below:

- Photoionization models with low column density ($N_H = 10^{22}$ cm^{-2}) are not able to reproduce the strong Fe II emission. We only recover the observed Fe II ratio in optical if we assume 10x solar abundance. In the NIR, even with this assumption of 10x solar abundance, we do not recover the observed estimate,
- For column density, $N_H = 10^{23}$ cm^{-2}, we recover favorable solutions in both optical and NIR Fe II intensity ratios that require abundances slightly above solar values, i.e., 2 $Z_\odot \leq Z \leq 5\ Z_\odot$,
- We also estimate the cloud densities from our modelling based on the recovery of the optical and NIR Fe II intensity ratios. Focusing on the cloud column density case, $N_H = 10^{23}$ cm^{-2}, the range of cloud densities for the optical: $10^{10.6}$ - $10^{12.4}$ cm^{-3}, while for the NIR: 10^{10} - $10^{11.9}$ cm^{-3}. This suggests that the density associated with the two emissions are overlapping, and
- Our results find that the new CLOUDY atomic dataset from Smyth et al. 2019 is more reliable to study the Fe II emission in the optical and NIR than the default Verner et al. 1999 dataset, especially for I Zw 1-like sources.

Acknowledgements. The authors thank the Brazilian Agencies: Agency of Coordenação de Aperfeiçoamento de Pessoal de Nível Superior (CAPES), and Conselho Nacional de Desenvolvimento Científico e Tecnológico (CNPq). We thank Dr. Marios Chatzikos and the CLOUDY team for giving us access to the developmental version.

References

Netzer, H., 2015, Annual Review of A&A, 53, 365-408
Padovani, P., et al., M., 2017, A&A Review, 25, 1-91
Collin, S., et. al., 2006, A&A, 456(1), 75-90
Panda, S., Marziani, P., and Czerny, B., 2019, ApJ, 882, 79
Blandford, R. D., and McKee, C. F., 1982, ApJ, 55, 419-439
Peterson, B. M., et al., 2004, ApJ, 613, 2, 682
Misty C. Bentz et al. 2013, ApJ, 767, 14
Du, Pu et al., 2015, ApJ, 806, 1, 22.
C. J. Grier et al., 2017, ApJ, 849, 146

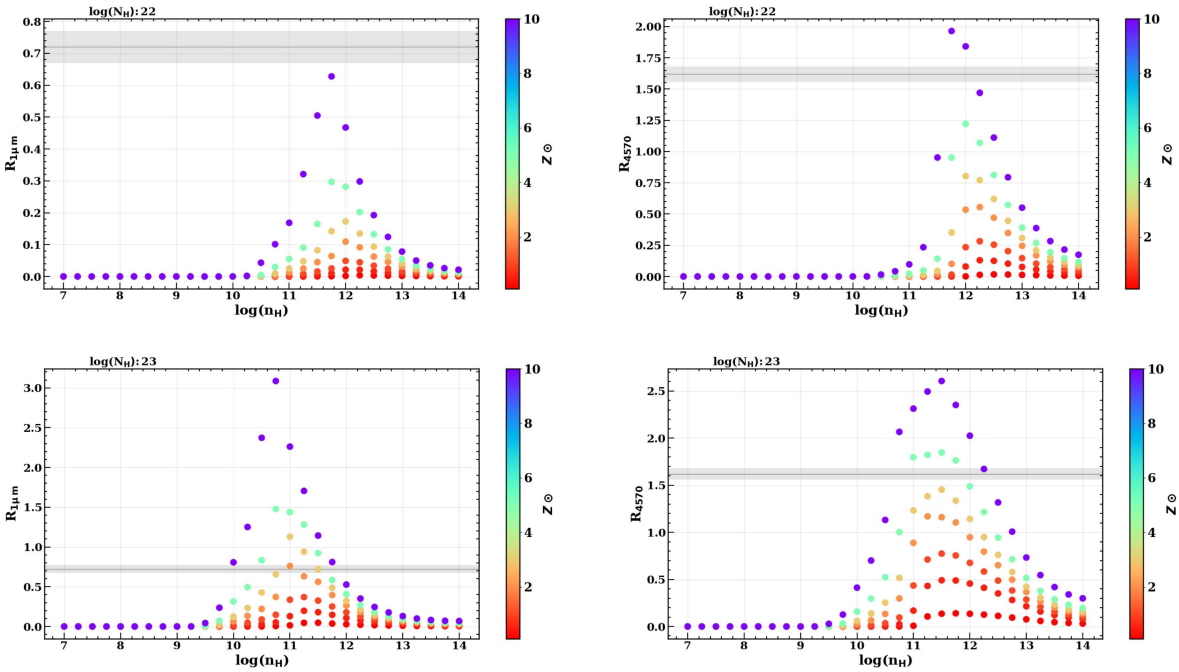

Figure 4. Diagnostic diagrams obtained from simulations. Upper row: $R_{1\mu m}$ and R_{4570} intensities vs cloud density n_H (in log-scale) for column density, $N_H = 10^{22}$ cm^{-2}. Lower row: The same scheme, but panels are shown for $N_H = 10^{23}$ cm^{-2}. In all cases, the color bars represent the abundance, ranging from 0.1 $Z_\odot$ to 10 $Z_\odot$.

Panda, S., et al., 2019, Frontiers Media SA, 6, 75
Daniel E. Vanden Berk, et. al., 200,1 ApJ, 122, 549
Glikman, Eilat and Helfand, David J. and White, Richard L., 2006, ApJ, 640, 579
Marinello, M. et al. 2020, MNRAS, 494, 3, 4187–4202
Wills, BEVERLEY J and Netzer, HAGAI and Wills, D, 1985, ApJ, 288, 94–116
Verner, E. M. et al., 1999, ApJS, 120, 101
Sigut, TAA. and Pradhan, Anil K., 2003, ApJS, 145, 1, 15
Hamann, Fred and Ferland, Gary, 1992, ApJ, 391, L53–L57
Baldwin, J. A., Ferland, G. J., Korista, K. T., Hamann, F., and LaCluyzé, A., 2004, ApJ, 615, 610
Martínez-Aldama, M, L. et al., 2021, ApJ, 918, 1, 29
Sarkar, A. et al., 2021, ApJ, 907, 1, 12
Boroson, Todd A. and Green, Richard F., 1992, ApJS, 80, 109–135
Vestergaard, Marianne and Wilkes, Belinda Jane, 2001, ApJS, 134, 1, 1
Tsuzuki, Y. et al., 2006, ApJ, 650, 1, 57
Kovačević-Dojčinović, Jelena and Popović, Luka Č, 2015, ApJS, 221, 2, 35
Dong, X., et al., 2010, ApJL, 721, 2, L143
Dong, X., et al., 2011, ApJ, 736, 2, 86
Kovačević, J., Popović, Luka Č and Dimitrijević, Milan S., 2010, ApJS, 189, 1, 15
Park, D., Barth, Aaron J., Ho, Luis C. and Laor, A., 2022, ApJS, 258, 2, 38
Sigut, TAA., and Pradhan, Anil K., 1998, ApJ, 499, 2, L139
Rodriguez-Ardila, A., et al., 2002, ApJ, 565, 1, 140
Sigut, TAA., Pradhan, Anil K., Nahar, Sultana N., 2004, ApJ, 611, 1, 81
Garcia-Rissmann, A., et al., 2012, ApJ, 751, 1, 7
Marinello, M and Rodríguez-Ardila, A., Garcia-Rissmann, A., Sigut, TAA., and Pradhan, AK., 2016, ApJ, 820, 2, 116
Rudy, Richard J., Mazuk, S., Puetter, RC., and Hamann, F., 2000, ApJ, 539, 1, 166
Riffel, R., Rodriguez-Ardila, A., and Pastoriza, Miriani Griselda, 2006, A&A, 457, 1, 61–70
Martínez-Aldama, M. L., et al., 2015, ApJS, 217, 1, 3
Panda, S., Martínez-Aldama, Mary Loli, Marinello, M., Czerny, B., and Marziani, P., and Dultzin, D., 2020, ApJ, 902, 1, 76
Panda, Swayamtrupta, 2021, Ats, 650, A154
Panda, S., Bon, E., Marziani, P., and Bon, N., 2022, Astronomische Nachrichten, 343(1-2), e210091
Korista, Kirk T. and Goad, Michael R., 2000, ApJ, 536, 1, 284–298
Goad, M. R. and Korista, K. T., 2014, MNRAS, 444, 1, 43–61
Panda, S., Czerny, B., Wildy, C., 2017, Frontiers Media SA, 4, 33
Véron-Cetty, M-P., Joly, M., Véron, P., 2004, A&A, 417, 2, 515–525
Huang, Ying-Ke, et al., 2019, ApJ, 876, 2, 102
Osterbrock, Donald E., Pogge, R. W., 1985, ApJ, 297, 166–176
Shen, Y. and Ho, Luis C., 2014, Nature, 513, 7517, 210–213
Rakshit, S., Stalin, CS., Kotilainen, J., 2020, ApJS, 249, 1, 17
Panda, S., Śniegowska, M., arXiv preprint arXiv:2206.10056, 2022
Panda, S., Polish Academy of Sciences, Institute of Physics, PhD thesis,sep, 2021
Barth, Aaron J., et al., 2013, ApJ, 769, 2, 128
Hu, C., et al., 2008, ApJ, 687, 1, 78–96
Bruhweiler, F. and Verner, E., 2008, ApJ, 675, 1, 83
Panda, S., Małek, K., and Śniegowska, M., and Czerny, B., 2019, IAU Proceedings, 15, S341, 297–298
Panda, S., Czerny, B., Done, C. and Kubota, A., 2019, ApJ, 875, 2, 133
Panda, S., 2021, Publications de l'Observatoire Astronomique de Beograd, 100, 333–338
Marziani, P. et al., 2022, ApJS, 261, 2, 30
Dias dos Santos, D., 2021, master dissertation, INPE
Smyth, RT and Ramsbottom, CA and Keenan, FP and Ferland, GJ and Ballance, CP, 2019, MNRAS, 483, 1, 654–663
Bautista, M. A., Fivet, V., Ballance, C., Quinet, P., Ferland, G., Mendoza, C., and Kallman, T. R., 2015, AAS, 808, 2, 174
Tayal, S. S. and Zatsarinny, O., 2018, Phys. Rev. A, 98, 1, 012706, 17
Ferland, G. J. and Chatzikos, M. and Guzmán, F. and Lykins, M. L. and van Hoof, P. A. M. and Williams, R. J. R. and Abel, N. P. and Badnell, N. R. and Keenan, F. P. and Porter, R. L. and Stancil, P. C., 2017, RMXAA, 53, 385-438
Kaspi, S., Smith, P. S., Netzer, H., Maoz, D., Jannuzi, B. T., & Giveon, U., 2000, ApJ, 533, 2, 631
Panda, S., Czerny, B., Adhikari, T. P., Hryniewicz, K., Wildy, C., Kuraszkiewicz, J., & Śniegowska, M., 2018, AAS, 866, 2, 115
Grevesse, N., Asplund, M., Sauval, A.J., and Scott, P., 2011, Canadian Journal of Physics, 89, 4, 327–331
Sulentic, J. W. and Zwitter, T. and Marziani, P. and Dultzin-Hacyan, D., 2000, ApJL, 536, 1, L5-L9
Marziani, P., Dultzin, D., Sulentic, J. W., Del Olmo, A., Negrete, C. A., Martínez-Aldama, M. L., D'Onofrio, M., Bon, E., Stirpe, N., and Giovanna. M., 2018, Frontiers Media S.A, 3, 5